

A NUMERICAL MODEL OF A CORONAL MASS EJECTION: SHOCK DEVELOPMENT WITH IMPLICATIONS FOR THE ACCELERATION OF GeV PROTONS

I. I. ROUSSEV,¹ I. V. SOKOLOV,¹ T. G. FORBES,² T. I. GOMBOSI,¹ M. A. LEE,² AND J. I. SAKAI³

Received 2004 January 14; accepted 2004 February 24; published 2004 March 10

ABSTRACT

The initiation and evolution of the coronal mass ejection, which occurred on 1998 May 2 in NOAA Active Region 8210, are modeled using a fully three-dimensional, global MHD code. The initial magnetic field for the model is based on magnetogram data from the Wilcox Solar Observatory, and the solar eruption is initiated by slowly evolving the boundary conditions until a critical point is reached where the configuration loses equilibrium. At this time, the field erupts, and a flux rope is ejected that achieves a maximum speed in excess of 1000 km s⁻¹. The shock that forms in front of the rope reaches a fast-mode Mach number in excess of 4 and a compression ratio greater than 3 by the time it has traveled a distance of 5 R_⊙ from the surface. For such values, diffusive shock acceleration theory predicts a distribution of solar energetic protons with a cutoff energy of about 10 GeV. For this event, there appears to be no need to introduce an additional acceleration mechanism to account for solar energetic protons with energies below 10 GeV.

Subject headings: acceleration of particles — MHD — shock waves — solar wind —
Sun: coronal mass ejections (CMEs) — Sun: magnetic fields

On-line material: mpeg animation

1. INTRODUCTION

Coronal mass ejections (CMEs), and the solar energetic particle (SEP) events associated with them, constitute one of the major hazards for spacecraft in the inner solar system. Particularly important in this regard are the high-energy (>100 MeV) protons, which can be accelerated within as short a span of time as 20 minutes after the onset of the CME. It has been proposed (e.g., Lee 1997; Reames 1999) that these particles are produced by a Fermi process (type A) at a shock that forms in front of the CME while it is still relatively close to the Sun (within 10 R_⊙). However, whether or not such a process is actually feasible has remained uncertain (Tsurutani et al. 2003), because of the lack of knowledge about the strength and location of the shock at such an early stage in the evolution of the CME. The prediction of shock properties so soon after the onset of the CME requires not only a realistic model of the magnetic field and plasma in the inner corona but also a realistic model of how the CME is initiated. To date, only limited progress has been made in realistically modeling CME initiation because most of the previous studies (Antiochos, DeVore, & Klimchuk 1999; Amari et al. 2000, 2003; Linker et al. 2001; Roussev et al. 2003a) involve idealized magnetic configurations. However, these do provide some of the essential physical insight needed to understand the nature of solar eruptions. In this Letter, we extend the previous studies by using the loss-of-equilibrium mechanism previously used by Amari et al. (1999), among others, within the framework of a global model of the solar magnetic field as it was observed by the Wilcox Solar Observatory on 1998 May 2. On this day, a CME associated with an X1.1/3B flare occurred in NOAA Active Region 8210 at 13:42 UT, which was associated with an SEP

event observed by the NOAA *GOES-9* satellite. A ground-level event was also observed by the CLIMAX neutron monitor (Lopate 2001).

A series of intense flares and CMEs, including homologous events, occurred in NOAA AR 8210 during the period from April through May of 1998 (Warmuth et al. 2000; Wang et al. 2002). The event we consider took place near the disk center (S15°, W15°), and the CME speed inferred from observations using the Large Angle and Spectrometric Coronagraph on the *Solar and Heliospheric Observatory* is in excess of 1040 km s⁻¹ (Pohjolainen et al. 2001). The total magnetic energy estimated from the EUV Imaging Telescope dimming volume during the eruption is ~2.0 × 10³¹ ergs (Wang et al. 2002). AR 8210 constituted a classic delta-spot configuration. The main spot in AR 8210 had a large negative polarity, and it appeared to rotate relative to the surrounding magnetic structures. Near the central spot, there was a sequence of cancellation events between it and newly emerging magnetic features of opposite polarity in the surrounding region (Sterling et al. 2001). This emergence and subsequent cancellation may have been responsible for triggering the eruption, since these processes have previously been proposed by various authors as possible factors leading to an eruption (see Feynman & Martin 1995, Wang & Sheeley 1999, and Lin, Forbes, & Isenberg 2001).

2. METHODOLOGY

The numerical model discussed below starts with a magnetic field obtained using the potential field source surface method (PFSSM; Altschuler et al. 1977). The spherical harmonic coefficients in the series are obtained from magnetogram data of the Wilcox Solar Observatory. They are derived using Carrington maps for rotations 1935 and 1936, so that in the composite synoptic map, AR 8210 appears at a heliographic latitude of -15° and a longitude of 185°. For our expansion order ($n_{\text{shc}} = 29$), the small-scale fields of AR 8210 are underresolved. While this does not pose any problem for obtaining a relatively realistic model of the magnetic field in the region of the corona where the CME shock forms, it does prevent us

¹ Center for Space Environment Modeling, University of Michigan, 2455 Hayward Street, Ann Arbor, MI 48109; iroussev@umich.edu, igorsok@umich.edu, tamas@umich.edu.

² Department of Physics and Institute for the Study of Earth, Ocean, and Space, University of New Hampshire, Durham, NH 03824; terry.forbes@unh.edu, marty.lee@unh.edu.

³ Laboratory for Plasma Astrophysics, Faculty of Engineering, Toyama University, Toyama 930-8555, Japan; sakaijun@eng.toyama-u.ac.jp.

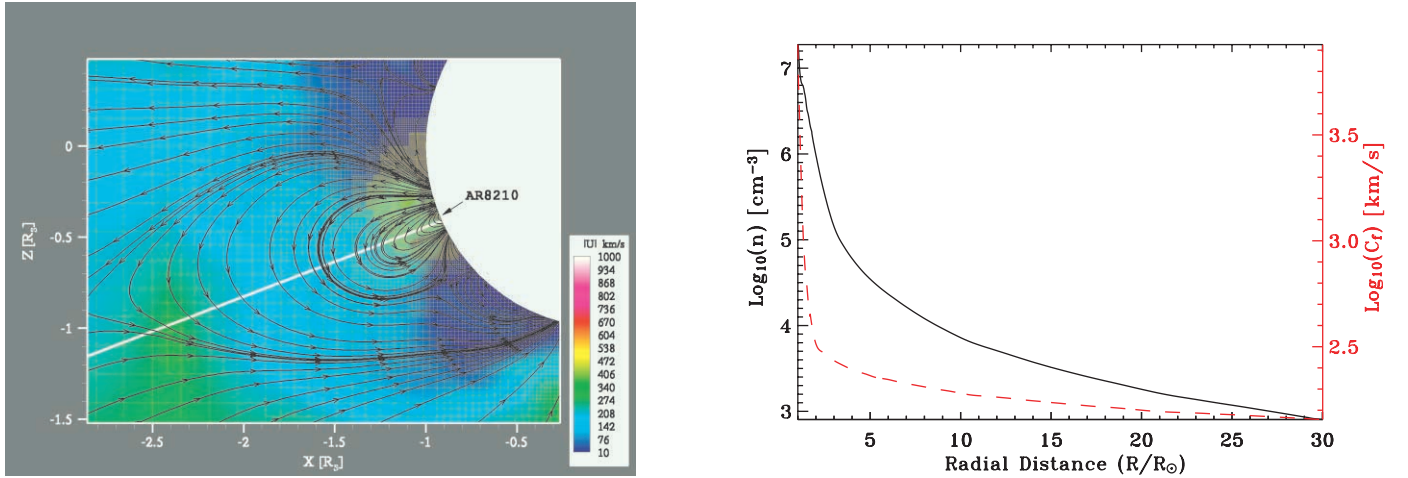


FIG. 1.—*Left:* Magnetic field configuration and flow pattern prior to the eruption (at $t = 230\tau_A$) in the $y = 0$ plane. *Right:* Curves of the number density and the fast-wave speed (red curve) as derived along the white line in the left panel at $t = 0$. The left panel of this figure is also available as an mpeg animation in the electronic edition of the *Astrophysical Journal*.

from obtaining an accurate description at the surface within the active region. Because of the low resolution of the field expansion, the central spot of AR 8210, which is observed to have a size of $\sim 2^\circ$ with a field strength of ~ -400 G, is spread over a region of $\sim 20^\circ$ with a field strength of ~ 35 G. Furthermore, the distribution of positive and negative polarities within the active region is so shifted that it is no longer possible to identify confidently which field structures in the expanded field correspond to the observed structures in the higher resolution magnetograms. Therefore, we are not able, in the work we discuss here, to model the detailed evolution of the field and flows at the solar surface. The best we can do with the given resolution is to evolve the low-resolution field in a way that is generally consistent with the motions observed in the high-resolution magnetograms but that is not consistent in detail. This procedure allows us to initiate a CME in a physically plausible manner, i.e., one that extracts magnetic energy stored in the corona by evolving the field to a point where a loss of equilibrium occurs. (In this simulation, nearly 16% of the magnetic energy stored in the corona at the time of eruption is converted into thermal and kinetic energy.) With this in mind, we do not claim that we model the actual surface magnetic field that is observed for AR 8210 but only that we model the coronal magnetic field above it at heights beyond about $1 R_\odot$. This is adequate for our purposes since our numerical study is targeted at reproducing the dynamics of the flux rope and the shock within the region from 1 to $20 R_\odot$ above the surface.

As in Roussev et al. (2003a, 2003b), the governing equations of a single-fluid, compressible magnetohydrodynamics (MHD) are solved using the BATS-R-US code. The computations are performed in a cubic box: $(-30 \leq x \leq 10, -20 \leq y \leq 20, -20 \leq z \leq 20) R_\odot$, using a nonuniform Cartesian grid. After two levels of uniform initial refinement, we applied seven more levels of body-focused refinement to achieve the finest grid near the Sun. In addition, there are two more levels of refinement applied in the vicinity of AR 8210 [centered at $\mathbf{R}_0(R, \theta, \phi) = (R_\odot, -14^\circ 81', 184^\circ 34')$], in order to better resolve the boundary motions that are applied. The grid structure can be seen in Figure 1 (*left panel*) and the accompanying mpeg animation. The total number of cells within the computational domain is 3,116,352; the smallest cell size corresponds to $4.883 \times 10^{-3} R_\odot$, while the largest cells have a size

of $2.5 R_\odot$. Once the flux rope is formed and starts erupting, we increase the resolution along the direction of rope propagation by adding 25% more cells (total of 3,890,944) through four levels of refinement (finest cells of size $0.156 R_\odot$).

The inner boundary conditions describe an “impenetrable” and highly conducting spherical inner body placed at $R = R_\odot$. During the time that the MHD solution is evolved toward a steady state solar wind, all the velocity components at the surface are fixed at zero (solar rotation is not applied), except for a small positive mass flow through the inner boundary, which is needed to balance the mass loss caused by the wind. Once a steady state wind flow is established, horizontal boundary motions are applied, which stress the magnetic field and build up currents in the region where the CME occurred. For the magnetic field, lined-tied boundary conditions are used so that the field remains frozen to the plasma, except in the regions where flux cancellation occurs. The pressure and mass density are fixed at the surface, and zero-gradient conditions are applied to all the physical variables at the six outer boundaries.

We use the empirical model presented in Roussev et al. (2003b) to evolve the MHD solution to a steady state solar wind, with a helmet-type streamer belt around the Sun. The initial magnetic field is calculated from the composite synoptic map described above using the PFSSM; the source surface is placed at $2.5 R_\odot$. Once the steady state is reached at $t = 0$, we begin inducing transverse motions at the surface localized to AR 8210.

Numerical techniques similar to ours have been extensively used in the past to create flux ropes and initiate CMEs in idealized, bipolar (Inhester, Birn, & Hesse 1992; Amari et al. 1999, 2000, 2003), and multipolar (Antiochos et al. 1999) magnetic configurations. For $t > 0$, at $\mathbf{R} = (R_\odot, \theta, \phi)$, we impose shear-type, foot-point motions that are localized along the polarity inversion line (PIL) of AR 8210 and tangential to the solar surface. We choose a velocity profile of the form

$$\mathbf{v}_s(\mathbf{R}; t) = v_m \kappa_s F_t^s \frac{\sin(\pi \kappa_s / \alpha) \mathbf{R}_0 \times \mathbf{R}}{\pi \kappa_s / \alpha R_\odot^2}, \quad (1)$$

where $F_t^s(t) = \min[t/(15\tau_A), 1]$ (with $\tau_A = R_\odot/v_A$ and a characteristic value of the Alfvén speed $v_A = \alpha B_{R_\odot} / \sqrt{\mu\rho} = 9250$ km

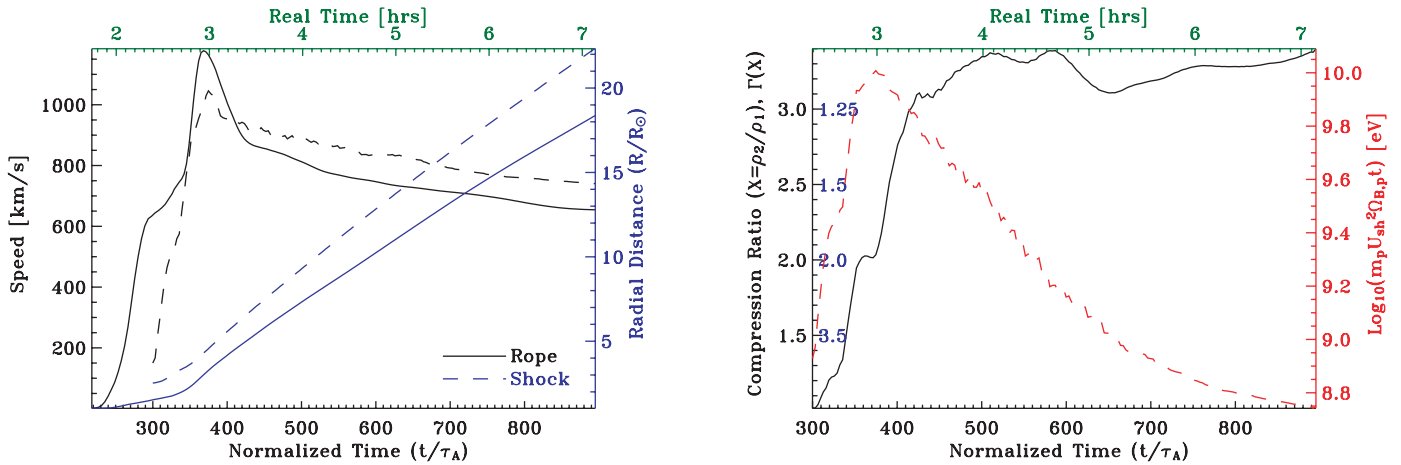


FIG. 2.—*Left*: Trajectory curves of the flux rope and the shock (*blue curves*) in the plane $y = 0$. The radial velocity of the rope and the shock are shown by the corresponding black curves. *Right*: Compression ratio of the shock and the proton cutoff energy predicted by diffusive shock acceleration theory. The interior labels along the left axis indicate the spectral index for the nonrelativistic particle flux used in the theory: $\Gamma = 0.5(X + 2)/(X - 1)$. Lower values of the index indicate a harder spectrum.

s^{-1}), $v_m = 0.01v_A$, $F_\sigma^s(\mathbf{R}) = \exp[-|\mathbf{R} - \mathbf{R}_v|^2/(2R_\sigma^2)]$, $\kappa_s(\mathbf{R}) = \min[\alpha, (B_R/B_{R_0} > 0)]$, and $\alpha = 0.25$. As above, \mathbf{R}_0 is the radius vector of the center of the spot, and $R_\sigma = 0.05 R_\odot$ is a free parameter used to set the gradient of the shearing motions away from the location $\mathbf{R}_v = (R_\odot, -16^\circ 31', 184^\circ 34')$, as prescribed by a Gaussian mask F_σ^s . Here B_R is the radial magnetic field at \mathbf{R} , B_{R_0} is the radial field strength at \mathbf{R}_0 , and μ and ρ have their usual meaning. The velocity profile given by equation (1) describes concentric vortex motions around the center of the spot of AR 8210. These motions are induced in a linear fashion from $t = 0$ to $t = 15\tau_A$, via the ramp-up function F_t^s , and are then maintained at a constant level of $0.01v_A$ up to $t = 311\tau_A$. Afterward, the shearing motions are smoothly diminished over a period of $15\tau_A$.

The dynamical consequences of flux cancellation are modeled by imposing converging motions (tangential to the solar surface) toward the PIL of AR 8210 of the kind

$$\mathbf{v}_c = v_m \kappa_c F_t^c F_\sigma^c \frac{\sin(\pi \kappa_c / \alpha)}{\pi \kappa_c / \alpha} \left(\frac{\mathbf{R}_0 \cdot \mathbf{R}}{R_\odot^2} \frac{\mathbf{R}}{R_\odot} - \frac{\mathbf{R}_0}{R_\odot} \right), \quad (2)$$

where $F_\sigma^c(\mathbf{R}) = \exp[-|\mathbf{R} - \mathbf{R}_c|^2/(2R_\sigma^2)]$ and $F_t^c(t) = \min[|t - 220\tau_A|/(15\tau_A), 1]$. Here $\mathbf{R}_c = (R_\odot, -19^\circ 31', 183^\circ 59')$ is the radius vector of the center of a Gaussian mask, F_σ^c , used to damp the converging motions away from the location given by \mathbf{R}_c . Unlike equation (1), here $\kappa_c(\mathbf{R}) = \min(\alpha, |B_R/B_{R_0}|)$; i.e., we consider both signs of B_R in constructing the velocity profile in space. The rest of the parameters in equation (2) are the same as in equation (1). The converging motions are induced in a manner similar to that of the shearing ones, using a linear ramp-up prescribed by F_t^c , from $t = 220\tau_A$ to $t = 235\tau_A$, and followed by a constant level of velocity magnitude of $0.01v_A$ up to $t = 311\tau_A$. These motions are smoothly diminished for $t > 311\tau_A$ over a period of $15\tau_A$.

3. CME INITIATION AND SHOCK DEVELOPMENT

During the phase of pure shear motions ($t \leq 220\tau_A$), the magnetic configuration evolves through a sequence of states close to equilibrium; this is ensured by the fact that the shear velocity is only 1% of v_A . During this phase, the magnetic energy monotonically increases (see also Amari et al. 1999, 2003).

The excess magnetic energy that is built in the sheared field at $t = 220\tau_A$ is 1.311×10^{31} ergs. (The magnetic energy summed over the entire domain at $t = 0$ is 1.255×10^{33} ergs.) As seen in the accompanying mpeg animation, the helmet streamer above AR 8210 evolves quasi-statically to a new equilibrium. Figure 1 (*left panel*) shows that AR 8210 appears as a quadrupolar-type magnetic configuration.

During the stage of converging motions ($t > 220\tau_A - 326\tau_A$), the cancellation of magnetic flux causes the magnetic energy to start declining, even though the rotation of the spot continues. The cancellation process (i.e., slow reconnection) leads to the formation of a flux rope, which increases in both size and twist with time. The outward force associated with this twist strengthens until eventually the overlying field is no longer able to confine the rope. The loss of confinement appears to happen catastrophically in much the same manner as occurred in the simulations of Amari et al. (1999), Linker et al. (2001), and Roussev et al. (2003a). The sudden force imbalance results in the outward acceleration of the flux rope over a few Alfvén timescales. The resulting trajectory of the flux rope in the $y = 0$ plane is shown in the left panel of Figure 2. By the time the boundary motions are turned off (at $t = 326\tau_A$), the flux rope has reached an altitude of nearly $1 R_\odot$ above the surface. As shown in Figure 2, the radial velocity of the flux rope increases up to a maximum value of $\sim 1190 \text{ km s}^{-1}$ at about $t = 365\tau_A$, when the rope has reached a distance of about $\sim 2 R_\odot$ above the surface. After this time, the speed declines, rapidly at first, but more slowly later on. The rapid decrease may be due to the formation of the current sheet, while the slow decrease is due to the snowplow effect; the mass of the material swept by the shock is comparable to (or greater than) that of the ejecta. A three-dimensional view of the eruption at $t = 382\tau_A$ is shown in Figure 3.

As the CME propagates through the ambient solar wind, a fast-mode shock forms ahead of it. The shock speed and its radial distance from the Sun, as measured along the direction $(-0.93, 0, -0.36)$, are also shown in the left panel of Figure 2 (see also the shock evolution along the corresponding white line in the accompanying mpeg animation). As seen in Figure 1 (*right panel*), the fast-wave speed sharply drops to 900 km s^{-1} at a distance of about $1.34 R_\odot$, followed by another factor of 6 decrease at $30 R_\odot$. Because of this sharp decrease

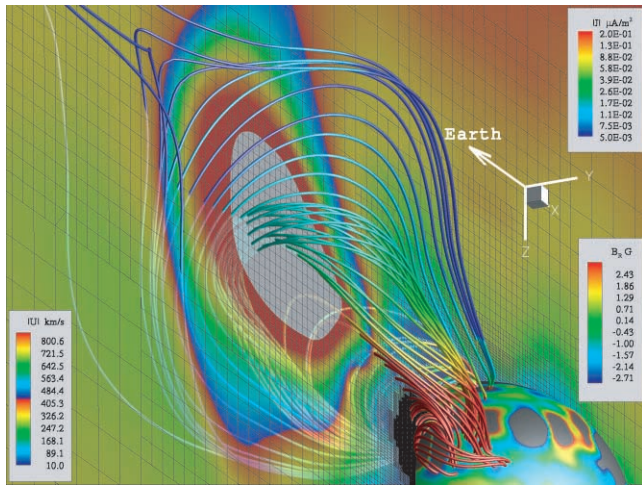


FIG. 3.—Three-dimensional view of the eruption at $t = 382\tau_A$. The solid lines are magnetic field lines; the false-color code shows the magnitude of the current density in units of $\mu\text{A m}^{-2}$ (see color legend at the top right). The magnitude of the flow velocity, in units of kilometers per second, is shown on a translucent plane given by $y = 0$ (see color legend to the left; note there are two cycles of the color code through the range of velocities shown). Values in excess of 1000 km s^{-1} are blanked and shown in light gray. The grid structure on this plane is also shown as the black frame. The inner sphere corresponds to $R = R_\odot$; the color code shows the distribution of the radial magnetic field in units of gauss (see color legend at the bottom right). Regions with radial field strength greater than 3 G are blanked and appear in gray.

so close to the Sun, the velocity of the ejecta quickly becomes supersonic (with respect to the fast-wave speed) locally, forming a shock that eventually reaches a compression ratio of about 3.4, as shown in the right panel of Figure 2. This ratio corresponds to a fast-mode Mach number of nearly 5. The increasing distance between the shock and the flux rope occurs because of the continual expansion of the flux rope with time. The right panel of Figure 2 also shows a high-energy cutoff for SEPs predicted on the basis of diffusive shock acceleration theory. The formula, shown on the right-hand side of the figure, is an upper limit derived from formula (6.7) in Axford (1981). This simple estimate, based on a comparison of the acceleration time with the shock wave propagation time, overestimates the actual cutoff by a factor of 2 or 3, depending on the shock's strength, the spectral index, and the angle of the upstream field, among other quantities, and does not involve a realistic model of turbulence. The cutoff reaches a

peak value of about 10 GeV within 1 hr of onset when the shock is still only at a distance of about $5 R_\odot$. This implies that the diffusive shock acceleration mechanism for this event could easily account for prompt, energetic particles below 10 GeV. The ability of the shock to produce such high energies in so short a time, by means of diffusive acceleration, is due to the rapid development of a high compression ratio (>3).

4. CONCLUSIONS

There has been some controversy in recent years about whether or not diffusive shock acceleration theory can account for the GeV particles observed early in SEP events (see Bulanov & Sokolov 1984 and the references therein; Kiplinger 1995; Tylka 2001; Reames 2002). The issue has been in doubt because there are conflicting demands put on the theory by the prompt appearance of such high-energy particles. To account for them, the theory requires that a strong shock with a large compression ratio occurs very early on and relatively close to the Sun ($<10 R_\odot$). However, near the Sun, the ambient Alfvén speed is so high, due to the strong magnetic fields there, that a strong shock is difficult to achieve. From the theoretical perspective, the problem of determining how the shock develops with time is further complicated by the absence of any generally accepted theory for how CMEs are triggered. How quickly the shock develops and strengthens depends very much on how it is driven by the erupting fields associated with the CME. By constructing a fully three-dimensional numerical model, which incorporates solar magnetic data and a loss-of-equilibrium mechanism, we have been able to determine that a shock can develop close to the Sun sufficiently strong to account for energetic particles up to 10 GeV. Whether similar results will be obtained for other events or other assumptions about the initiation mechanism remains to be seen. However, if they are, then it would seem likely that diffusive shock acceleration alone accounts for the GeV particles in SEP events.

The authors thank S. Antiochos, G. Fisher, J. R. Jokipii, Y. Liu, B. C. Low, J. Luhmann, M. Velli, and an unknown referee for their comments. This research work was supported by the following grants: DoD MURI F49620-01-1-0359, NSF ACI-9876943, NSF ATM-0325332, NASA NAG5-9406, 8228, 10977, and 10852, NSF ATM-0091527, and NSF ATM-0327512.

REFERENCES

- Altschuler, M. D., Levine, R. H., Stix, M., & Harvey, J. 1977, *Sol. Phys.*, 51, 345
 Amari, T., Luciani, J. F., Aly, J. J., Mikić, Z., & Linker, J. 2003, *ApJ*, 585, 1073
 Amari, T., Luciani, J. F., Mikić, Z., & Linker, J. 1999, *ApJ*, 518, L57
 ———. 2000, *ApJ*, 529, L49
 Antiochos, S. K., DeVore, C. R., & Klimchuk, J. A. 1999, *ApJ*, 510, 485
 Axford, W. I. 1981, *Proc. 17th Int. Cosmic Ray Conf. (Paris)*, 12, 155
 Bulanov, S. V., & Sokolov, I. V. 1984, *Soviet Astron. Lett.*, 10, 247
 Feynman, J., & Martin, S. F. 1995, *J. Geophys. Res.*, 100, 3355
 Inhester, B., Birn, J., & Hesse, M. 1992, *Sol. Phys.*, 138, 257
 Kiplinger, A. L. 1995, *ApJ*, 453, 973
 Lee, M. A. 1997, *Geophys. Monogr.*, 99, 227
 Lin, J., Forbes, T. G., & Isenberg, P. A. 2001, *J. Geophys. Res.*, 106, 25053
 Linker, J., Lionello, R., Mikić, Z., & Amari, T. 2001, *J. Geophys. Res.*, 106, 25165
 Lopate, C. 2001, *Proc. 27th Int. Cosmic Ray Conf. (Hamburg)*, 8, 3398
 Pohjolainen, S., et al. 2001, *ApJ*, 556, 421
 Reames, D. V. 1999, *Space Sci. Rev.*, 90, 413
 ———. 2002, *ApJ*, 571, L63
 Roussev, I. I., Forbes, T. G., Gombosi, T. I., Sokolov, I. V., DeZeeuw, D. L., & Birn, J. 2003a, *ApJ*, 588, L45
 Roussev, I. I., et al. 2003b, *ApJ*, 595, L57
 Sterling, A. C., Moore, R. L., Qiu, J., & Wang, H. 2001, *ApJ*, 561, 1116
 Tsurutani, B., Wu, S. T., Zhang, T. X., & Dryer, M. 2003, *A&A*, 412, 293
 Tylka, A. J. 2001, *J. Geophys. Res.*, 106, 25333
 Wang, T., Yan, Y., Wang, J., Kurokawa, H., & Shibata, K. 2002, *ApJ*, 572, 580
 Wang, Y.-M., & Sheeley, N. R., Jr. 1999, *ApJ*, 510, L157
 Warmuth, A., Hanslmeier, A., Messerotti, M., Caccianti, A., Moretti, P. F., & Otruba, W. 2000, *Sol. Phys.*, 194, 103